RSC Advances

PAPER

View Article Online
View Journal | View Issue

Cite this: *RSC Adv.*, 2018, **8**, 25445

Porous Fe^0/C ceramsites for removal of aqueous Pb(II) ions: equilibrium, long-term performance and mechanism studies†

Pingfeng Fu, * Xiaofeng Lin and Zihao Chen

This study reports the equilibrium, long-term performance and mechanisms in removing Pb(II) ions by metallic iron/carbon (Fe^0/C) ceramsites (FCC). The Pb(II) removal equilibrium data was analyzed using the Langmuir, Freundlich and Dubinin–Radushkevich isotherms. At the FCC dosage of 1.14 g L^{-1}, 95.97% of Pb(II) ions were removed from 50 mg L^{-1} Pb(II) solution at initial pH 6.0. The Langmuir isotherm could fit well with the data at initial pH 3.0 with a maximum monolayer adsorption capacity of 112.36 mg g^{-1} at 25 °C, while the data obtained at initial pH 6.0 could be described by the Freundlich model, indicating multilayer adsorption of Pb species on the FCC. Column tests demonstrated that FCC achieved the highest Pb(II) removal of 65.86% after 12 days' run compared to 32.35% for Fe^0/activated carbon couples and only 1.24% for activated carbon. The X-ray diffraction and X-ray photoelectron spectroscopy analysis revealed that the PbO (dominant Pb species), Pb^0, asisite and plumbojarosite appeared after Pb(II) removal. Scanning electron microscopy with energy dispersive X-ray spectroscopy showed that PbO particles with numerous structures were deposited on the FCC surface in a high amount. The decrease of the Fe/C mass ratio from 7.5 : 1 to 0.298 : 1 revealed that microscale Fe^0 could been readily corroded by forming galvanic couples between Fe^0 and carbon. The mechanisms of Pb(II) removal by the FCC were proposed.

Received 16th June 2018
Accepted 10th July 2018

DOI: 10.1039/c8ra05164j

rsc.li/rsc-advances

1. Introduction

Nanoscale zero-valent iron (nZVI) is very effective in the removal of heavy metal ions with numerous pathways, including adsorption, complexation, (co-)precipitation and chemical reduction.[1–3] Although the nZVI exhibits high efficiencies in removing heavy metal ions, some drawbacks related to ultrafine particle size are challenging the suitability of nZVI. The decrease of particle size is coupled with rapid corrosion of metallic iron (Fe^0) and the formation of corrosion products, which results in particle cementation and short service time for nZVI.[4,5] Moreover, the high redox reactivity of nZVI makes it potentially harmful to living organisms such as lung cells.[6]

Microscale Fe^0 materials (iron scraps or sponge iron) are widely applied in wastewater and groundwater treatment by coupling with non-expansive materials such as sands and pumices.[6,7] However, in comparison with nZVI, μm and mm sized Fe^0 particles show much lower reactivity due to slow corrosion of Fe^0 in the Fe^0/H_2O system. Thus, some methods such as using bimetallics, ultrasound enhancement and combining activated carbon (AC) with Fe^0 materials have been attempted to increase removal efficiencies of various pollutants.[8–10] Among these alternatives, by coupling Fe^0 with AC, the corrosion of Fe^0 can be remarkably enhanced as iron–carbon microelectrolysis reactions occur by forming microscopic galvanic cells.[10–12] The electrons of galvanic cells are supplied by the Fe^0 corrosion, and half-cell reactions can be represented as eqn (1)–(3). The microelectrolysis process has been widely attempted to degrade organic pollutants,[12,13] but its application in removing heavy metal ions is relatively rare. In previous reports, high removal efficiencies of heavy metals have been achieved by Fe^0/AC couples. Dou *et al.*[10] found that Fe^0/AC couples were capable of removing 100% of aqueous As(v), whereas only about 60% and 5% of As(v) was removed by Fe^0 and AC, respectively. Yuan *et al.*[11] observed that Fe^0/AC-ceramsites achieved higher Pb(II) removal (99.5%) compared to AC-ceramsite (7.8%) and Fe^0-ceramsite (39.6%).

Anode (Fe^0):

$$Fe - 2e^- \rightarrow Fe^{2+},\ E^0\ (Fe^{2+}/Fe) = -0.44\ V \quad (1)$$

Cathode (AC):

Acid with oxygen: $O_2 + 4H^+ + 4e^- \rightarrow 2H_2O,\ E^0(O_2/H_2O) = +1.23\ V$ (2)

School of Civil and Resources Engineering, University of Science and Technology Beijing, Beijing 100083, China. E-mail: pffu@ces.ustb.edu.cn; Fax: +86 10 82385795; Tel: +86 10 62332902

† Electronic supplementary information (ESI) available. See DOI: 10.1039/c8ra05164j

Neutral to alkaline with oxygen: $O_2 + 2H_2O + 4e^- \rightarrow 4OH^-$, $E^0(O_2/OH^-) = +0.40$ V (3)

Nevertheless, most of reported Fe^0/AC couples were just formed by physically mixing Fe^0 powders and granular AC in water.[10,14] As the corrosion of Fe^0 is a volumetric expansion process, mixed Fe^0/AC filters in flow-through treating systems may clog after a short service time.[15] Gelatinous iron hydroxides can cement Fe^0 and AC particles, resulting in the compaction of fillings.[16] By integrating Fe^0 materials and AC in one pellet, these disadvantages may be avoided. The microelectrolysis process using integrated Fe^0/AC filters has been applied in degradation of organic pollutants with advantages of low pressure drop and long-term operation.[13,17] However, these Fe^0/AC microelectrolysis filters are rarely applied in removing heavy metals. Moreover, Fe^0/AC couples should be costly due to the usage of commercial Fe^0 powders and AC although AC can be fabricated from various solid wastes.[18–20] Therefore, the development of cost-effective and integrated microelectrolysis filter from cheap raw materials is very expected, and its evaluation of heavy metal removal is necessary.

Lead in the wastewater is extremely toxic to human beings and ecosystems.[21–23] Lead can damage nervous systems, kidneys, reproductive systems and other organs.[24] Therefore, it is of great concern for developing cost-effective technologies to treat lead contaminated wastewaters.[25]

In this work, porous Fe^0/C ceramsite (FCC), a novel microelectrolysis filter, has been prepared by the direct reduction roasting of magnetite, coal and paper mill sludge. Metallic iron (Fe^0) generated from *in situ* reduction of magnetite, and carbon particles achieved from the carbonization of coal, are served as anode and cathode of the microelectrolysis filter, respectively. Compared to reported Fe^0/AC couples or filters, the FCC in this work is cost-effective and eco-friendly by using cheap raw materials and solid waste (paper mill sludge). The objectives of this work are (1) to investigate the effect of initial solution pH on Pb(II) removal by the FCC; (2) to analyze equilibrium data of Pb(II) removal to understand adsorption characteristics of the FCC; (3) to evaluate long-term performance of Pb(II) removal with column tests; (4) to propose Pb(II) removal mechanisms by the FCC with FESEM/EDX, XRD and XPS analysis.

2. Materials and methods

2.1 Materials

The magnetite with Fe content of 66.32% was used as the source of metallic iron. The paper mill sludge was collected from the MCC Paper Yinhe Company of China. The contents of volatiles, fixed carbon and ashes of dried sludge were 42.56%, 2.23% and 55.21%, respectively. The coal with fixed carbon of 58.23% was served as the reducing agent and precursor of cathode. Lead nitrate ($Pb(NO_3)_2$), sodium silicate ($Na_2SiO_3 \cdot 9H_2O$), Fe^0 powders and quartz sands were purchased from Sinopharm Chemical reagent Co. Ltd. (China). All reagents used were of analytical grade (AR).

Fe^0 powders were available as fillings with a particle size of between 0.5 and 2.0 mm. The Fe content as specified by the supplier was 97.46%. Quartz sands with SiO_2 content of 98.23% were used with a particle size between 0.65 and 0.85 mm. Cylindrical activated carbon (AC) with 3 mm diameter and 4–6 mm height was received from Jinling Environmental Technology Co. Ltd. (China). The AC prepared from coal had a specific surface area of 864.25 $m^2\ g^{-1}$. Fe^0 powders, quartz sands and AC were used without further treatment.

2.2 Preparation of Fe^0/C ceramsites

Fig. S1† (see in the ESI) showed the fabrication procedure of Fe^0/C ceramsites (FCC). The magnetite, coal, paper mill sludge and sodium silicate were mixed with a mass ratio of 55 : 14 : 25 : 6. By adding 10% deionized water, wet mixtures were pressed into spheroidal pellets in a pelletizer. Then wet pellets were dried to constant weight at 105 °C in an oven. When the roasting temperature reached 1200 °C, dried pellets in a graphite crucible were transferred into a muffle furnace, and sintered at 1200 °C for 120 min at an oxygen deficient reduction atmosphere. After the calcination, the pellets were cooled down to 300 °C in the furnace, and then taken out to further cool down in air. Finally, porous Fe^0/C ceramsites as shown in Fig. S2† were fabricated.

2.3 Batch experiments

By dissolving appropriate amount of $Pb(NO_3)_2$ in deionized water, the stock solution with Pb(II) concentration of 800 mg L^{-1} was prepared, then diluted to obtain desired concentrations. To perform batch tests, spheroidal FCC was firstly crushed and sieved to obtain FCC powders with a size of <0.5 mm. 0.798 g FCC was added into 700 mL Pb(II) solution in a 1000 mL conical flask. The flask was stirred in a thermostated orbital shaker at 25 °C and 190 ± 5 rpm to perform adsorption experiments. The effect of initial pH on Pb(II) removal was performed at the Pb(II) concentration of 50 mg L^{-1} and FCC dosage of 1.14 g L^{-1}. The initial pH was chosen as 2.0, 3.0, 4.0, 5.0 and 6.0, respectively. The pH was adjusted by adding 0.1 M HCl or 0.1 M NaOH solution. The adsorption equilibrium tests were conducted at initial pH of 3.0 and 6.0 with FCC dosage of 1.14 g L^{-1}. The contact time was 150 min to achieve the adsorption equilibrium. The adsorption capacity q_t and q_e were calculated by following expressions:

$$q_t = \frac{C_0 - C_t}{W} \times V \quad (4)$$

$$q_e = \frac{C_0 - C_e}{W} \times V \quad (5)$$

where q_t and q_e (mg g^{-1}) were the amount of Pb(II) ions adsorbed on the FCC at time t (min) and equilibrium, respectively; C_0, C_t and C_e were the Pb(II) concentration (mg L^{-1}) at initial, time t and equilibrium, respectively; V was the solution volume (L), and W was the added amount (g) of the FCC.

2.4 Column experiments

Glass columns of 25 mm inner diameter and 250 mm length were used. A porous glass distributor was fixed at the bottom.

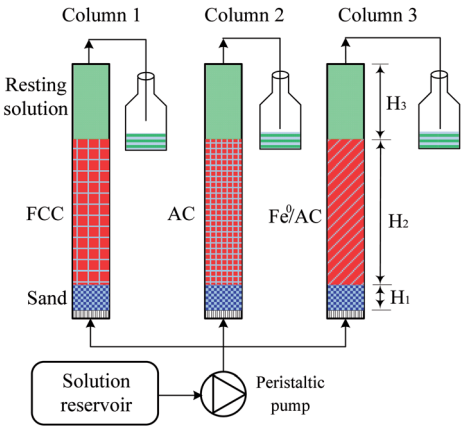

Fig. 1 Schematic diagram of column experiment design.

From the bottom to the top, the columns were packed as following: (1) fine sands ($H_1 = 20$ mm), (2) a reaction zone ($H_2 = 150$ mm), and (3) resting solution ($H_3 = 80$ mm). The reaction zones were packed with 74.46 g of spheroidal FCC in column 1, 40.41 g of cylindrical AC in column 2, and 5.08 g AC, 38.11 g Fe^0 powders and 58.03 g sands in column 3, respectively. For the comparison, the weights of metallic iron and carbon in columns 1 and 3 were set to be same, and sands were filled in column 3 to make same height of reaction zone in column 1 and 3.

Fig. 1 showed the schematic diagram of column experiments. 50 mg L^{-1} Pb(II) solution with initial pH 6.0 was pumped upwards into the columns from a solution reservoir using a peristaltic pump (BT-300CA/153Y). Tygon tubes were used to connect the solution reservoir, pump, column and outlet. The column experiments were conducted at room temperature (24 ± 3 °C) for 12 days. A stable flow rate of 2.0 mL min^{-1} was maintained throughout the experiment. In batch and column tests, aqueous samples were firstly filtered through a micro filter with a pore size of 0.45 μm. The Pb(II) concentration was then determined by inductively coupled plasma atomic emission spectrometer (ICP-AES, IRIS Intrepid II XSP).

2.5 Analysis and characterization

The carbon content of Fe^0/C ceramsites (FCC) was detected with a high frequency combustion and infrared absorption method. The content of metallic iron in the FCC was determined according to Chinese Standard GB/T 6730-1986. The compressive strength of FCC was determined by an intelligent particle strength analyzer (DL-III, China).

The morphology and elemental mapping EDX of fabricated FCC were performed by a scanning electron microscope equipped with an energy-dispersive X-ray spectrometer (SEM/EDX, Carl Zeiss EVO18). But the morphologies and element compositions of the FCC after Pb(II) removal were obtained by a field emission scanning electron microscope equipped with an energy-dispersive X-ray spectrometer (FESEM/EDX, JSM-6701F/Thermo NS7). The crystalline phases of the FCC before and after Pb(II) removal were characterized *via* X-ray diffraction (XRD, Dmax-RD12 kW, Rigaku) under the conditions of 40 kV, 100 mA and Cu Kα radiation. The data were collected with a 2θ range of 10–90°. The XPS analysis was performed with an X-ray photoelectron spectrometer (Kratos AXIS Ultra DLD) using a monochromatic Al Kα radiation. The binding energy was recorded with a reference to C 1s peak at 284.6 eV of the surface adventitious carbon. XPS data was analyzed using the XPSPEAK41 software. Prior to the FESEM/EDX, XRD and XPS analysis, FCC samples obtained after Pb(II) removal for 12 days were dried in a N_2 atmosphere at 105 °C for 2 h.

2.6 Equilibrium modeling

In this work, the equilibrium data of Pb(II) removal was analyzed in terms of the Langmuir, Freundlich and Dubinin–Radushkevich isotherms, respectively. The Langmuir isotherm equation in linear form is:

$$\frac{C_e}{q_e} = \frac{C_e}{q_m} + \frac{1}{q_m K_L} \quad (6)$$

where q_m (mg g^{-1}) is a maximum adsorption capacity of Pb(II) ions at complete monolayer coverage, and K_L (L mg^{-1}) is a Langmuir constant related to the adsorption energy. The Langmuir isotherm assumes the monolayer coverage of absorbent surface.[26–28]

The linear form of Freundlich model can be written as:

$$\log q_e = \log K_F + 1/n \log C_e \quad (7)$$

where K_F ($mg^{1-(1/n)}$ $L^{1/n}$ g^{-1}) is a measure of the adsorption capacity of adsorbent, and $1/n$ is the Freundlich exponent related to adsorption intensity. The Freundlich isotherm is generally applied both monolayer (chemisorption) and multilayer (physisorption) adsorption on heterogeneous surfaces, and the surface sites of the adsorbent have different binding energies.[29–32]

The Dubinin–Radushkevich (D–R) isotherm is applied to evaluate if the nature of adsorption is physical or chemical. The linear form of D-R isotherm is written as:

$$\ln q_e = \ln q_m - \left(\frac{RT}{2E}\right)^2 \left[\ln\left(1 + \frac{1}{C_e}\right)\right]^2 \quad (8)$$

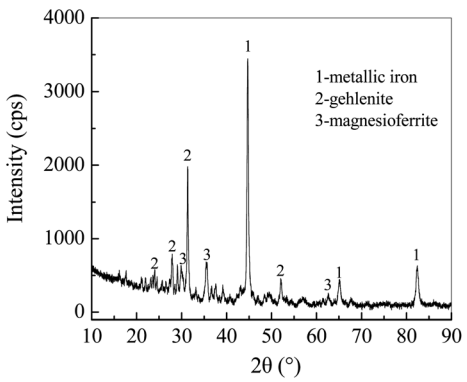

Fig. 2 XRD pattern of fabricated Fe^0/C ceramsites.

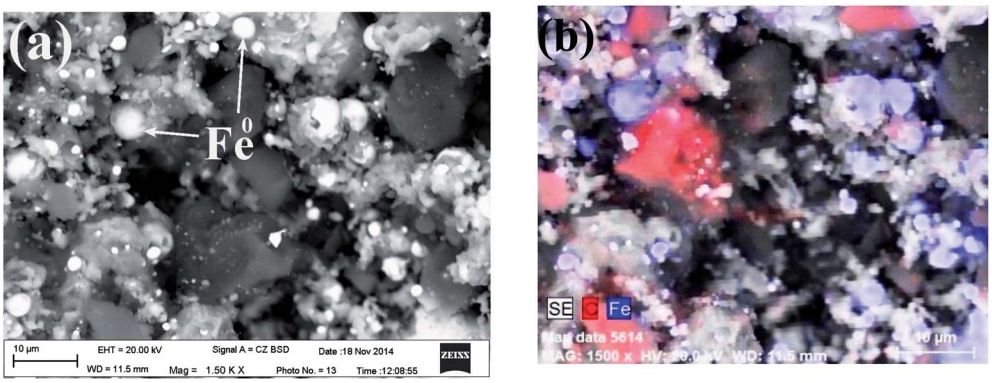

Fig. 3 SEM image (a) and elemental EDX mapping image (b) of Fe^0/C ceramsites.

where q_{max} (mol g^{-1}) is the theoretical saturation capacity, C_e (mol L^{-1}) is the Pb(II) concentration at equilibrium, R (8.314 J mol^{-1} K^{-1}) is the universal gas constant, T (K) is the absolute temperature, E (kJ mol^{-1}) is the mean free energy of adsorption.[33–35]

3. Results and discussion

3.1 Characterization of Fe^0/C ceramsites

The XRD pattern of Fe^0/C ceramsites (FCC) in Fig. 2 showed that the peaks with a 2θ degree at 44.62°, 65.23°, 82.43° corresponded to (110), (200) and (211) lattice planes of metallic iron (Fe^0), respectively. No diffraction peaks assigned to magnetite were found, revealing the complete reduction of magnetite to Fe^0 in the direct reduction roasting.[36]

As shown in Fig. 3(a), round white particles were *in situ* generated Fe^0 particles with a size of less than 5 μm. The elemental EDX mapping image (Fig. 3(b)) revealed that light blue particles (Fe^0) were uniformly distributed on the FCC surface, and red particles (carbon) with a size of around 10 μm were closely contacted with Fe^0 particles. The close distribution of anode (Fe^0) and cathode (carbon) in the FCC can facilitate electron transfer in galvanic cells. As summarized in Table S1,† the content of metallic iron in the FCC reached 52.18% with a Fe/C mass ratio of 7.5 : 1. Higher content of metallic iron may lead to longer reaction term of iron–carbon micro-electrolysis.[10,37] As illustrated in Fig. 3, numerous pores or fractures in the FCC were observed, which resulted in a large porosity of 46.37 vol% (Table S1†). In previous report of fly ash supported zero-valent iron prepared by direct reduction with coke, the Fourier transform infrared spectroscopy (FTIR) analysis demonstrated the existence of surface functional groups such as –OH, carboxyl and C–H groups.[38] Thus, these functional groups might also appear on FCC surface due to similar fabrication method. The compressive strength of the FCC reached 53.9 MPa, and the high mechanical strength should be attributed to the generation of gehlenite ($2CaO \cdot Al_2O_3 \cdot SiO_2$) after high temperature reduction roasting.

3.2 Effect of initial pH on Pb(II) removal

The solution pH strongly influences the Pb(II) removal as it can affect the Fe^0 corrosion, surface charge of Fe^0/C ceramsite (FCC) and speciation of Pb(II). As shown in Fig. 4(a), the Pb(II) removal rapidly increased in the first 10 min, and then gradually incremented until an adsorption equilibrium reached after 60 min. As initial pH rose from 2.0 to 6.0, the removal rate increased from 74.94% to 95.97%, showing the pH-sensitivity in Pb(II) removal by the FCC. The pH-sensitivity in removing heavy metal

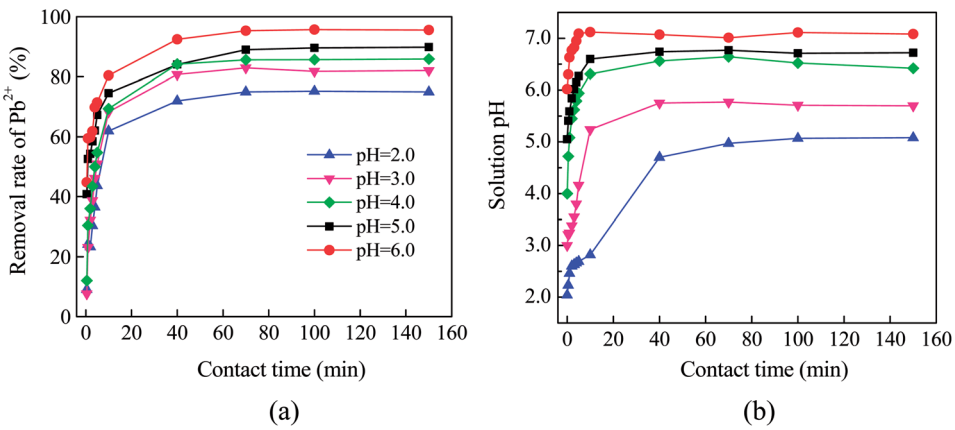

Fig. 4 Effect of initial pH on the Pb(II) removal by Fe^0/C ceramsites (a) and variation of solution pH with contact time (b).

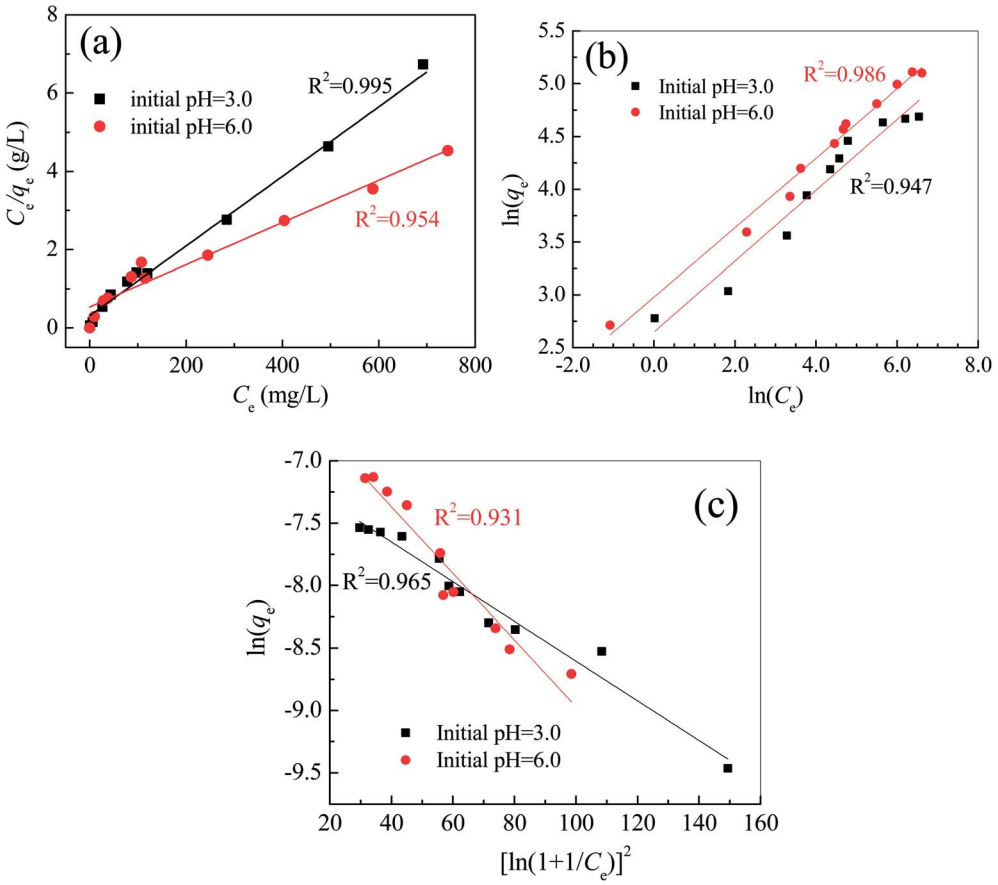

Fig. 5 Linearized fitting of Langmuir (a), Freundlich (b) and Dubinin–Raduskevich (c) isotherms for the Pb(II) removal by Fe^0/C ceramsites at 25 °C.

ions was also observed by other zero-valent iron sorbents.[1,2,11] The corrosion of Fe^0 can readily release active Fe(II) and Fe(III) ions, which are further hydrolyzed to generate iron hydroxides (*e.g.*, $Fe(OH)_3$) at the pH > 4.0. The iron hydroxides can effectively remove heavy metal ions by the adsorption, ion exchange and co-precipitation.[1,13]

As shown in Fig. 4(b), the solution pH increased as the removal process proceeded. The equilibrium pH had ascended up to 5.08, 5.71, 6.42, 6.72 and 7.08 from initial pH of 2.0, 3.0, 4.0, 5.0, 6.0, respectively. Other authors also observed the increase of solution pH while immersing Fe^0/AC couples in water.[11,13,14] The half-cell reactions given in eqn (2) and (3) showed the consumption of H^+ ions or release of OH^- ions into solution, resulting in the increase of solution pH. Additionally, the dissolution of surface substances and ion exchange of surficial OH^- with metal ions also contributed to the elevation of solution pH for Fe^0 sorbents.[39,40]

As the pH can significantly change the speciation of Pb(II), the increase of solution pH may lead to the precipitation of $Pb(OH)_2$. In this case, for the $Pb(NO_3)_2$ solution with Pb(II) concentration of 50 mg L^{-1}, the precipitation may occur at pH = 6.67 ($K_{sp,Pb(OH)_2} = 1.2 \times 10^{-15}$ at 25 °C). As shown in Fig. 4(b),

Table 1 Regression coefficients and isotherm parameters for Pb(II) removal at initial pH 3.0 and 6.0 by Fe^0/C ceramsites at 25 °C

Isotherm	Parameters	pH = 3.0	pH = 6.0
Langmuir $\frac{C_e}{q_e} = \frac{1}{q_{max}K_L} + \frac{1}{q_{max}}C_e$	$q_{m,cal}$ (mg g^{-1})	112.36	185.53
	$q_{m,exp}$ (mg g^{-1})	106.64	159.68
	K_L (L mg^{-1})	0.0285	0.00987
	R^2	0.995	0.954
Freundlich $\ln q_e = 1/n \ln C_e + \ln K_F$	K_F ($mg^{1-(1/n)}$ $L^{1/n}$ g^{-1})	13.41	19.87
	$1/n$	0.271	0.383
	R^2	0.947	0.986
Dubinin–Raduskevich $\ln q_e = \ln q_{max} - \left(\frac{RT}{2E}\right)^2 \left[\ln\left(1 + \frac{1}{C_e}\right)\right]^2$	q_{max} (mol g^{-1})	0.90×10^{-3}	1.84×10^{-3}
	E (kJ mol^{-1})	13.89	7.68
	R^2	0.965	0.931

Table 2 Comparison studies of maximum monolayer adsorption of Pb(II) ions on various adsorbents and their experimental conditions

Adsorbents	q_m (mg g^{-1})	Experimental conditions			Reference
		Sorbent dosage (g mL^{-1})	pH	T (K)	
Mn_3O_4-coated activated carbon	59.52	0.2/200	5.0	303	49
Activated carbon from apple pulp	15.96	0.1/25	5.0	298	50
Iron-activated carbon nanocomposite	121.9	0.05/50	6.0	298	29
Cyclone steel dust	39.8	0.1/50	5.0	298	51
Modified carbon nanotubes	100.0	0.2/1000	6.0	303	52
Chitosan schiff's base@Fe_3O_4	62.5	0.5/25	5.0	303	53
Chitosan functionalized magnetic particles	498.6	0.1/100	6.0	303	54
Sulfuric acid modified *Caryota urens* seeds	93.7	0.5/100	5.0	303	55
Microalga *Rhizoclonium hookeri*	81.7	0.1/100	4.5	298	56
Fe^0/C ceramsites	112.36	0.114/100	3.0	298	This work

the precipitation of $Pb(OH)_2$ was expected while initial pH was higher than 4.0. Especially, the precipitation would greatly contribute to the Pb(II) removal at initial pH 6.0 since the equilibrium pH had increased up to 7.08.

3.3 Adsorption isotherms

The equilibrium data of Pb(II) removal by the FCC was given in Fig. S3†. The linearized fitting of Langmuir, Freundlich and Dubinin–Raduskevich isotherms was shown in Fig. 5 with isotherm parameters summarized in Table 1. The regression coefficients of three models indicated that the data at initial pH 3.0 could be fitted well with the Langmuir isotherm, but the Freundlich equation was the best to fit the data at initial pH 6.0. The exponent of $1/n$ between $0 < 1/n < 1.0$ represented that the adsorption of Pb(II) on the FCC well obeyed the Freundlich model.[1,29,41] In the Langmuir model, the calculated maximum adsorption capacity ($q_{m,cal}$) was close to experimental one ($q_{m,exp}$) at initial pH 3.0, but the $q_{m,cal}$ was much higher than the $q_{m,exp}$ at initial pH 6.0. The parameter K_L represents the interaction intensity between the adsorbent and the adsorbate.[42,43] The larger value of K_L at initial pH 3.0 indicated the higher affinity of Pb species on the FCC surface at pH 3.0 than 6.0. The results demonstrated the monolayer coverage of Pb species on the FCC at initial pH 3.0, but multilayer adsorption occurred on FCC surface at initial pH 6.0.[29] The precipitation of lead oxides (hydroxides) on the FCC (physisorption) might occur at initial pH 6.0, which resulted in multilayer adsorption of Pb species.

In the Dubinin–Radushkevich model, the magnitude of E is used to reveal the mechanism of adsorption reactions.[44–46] An adsorption process is dominated by chemisorption/ion exchange if E is in the range of 8–16 kJ mol^{-1}, otherwise physical forces may affect the adsorption in the case of E < 8 kJ mol^{-1}.[33,47] Therefore, in this case, the Pb(II) removal by the FCC at initial pH 3.0 was controlled by the chemisorption/ion exchange as the E value reached 13.89 kJ mol^{-1}. However, physical forces might contribute to Pb(II) removal at initial pH 6.0 as the E value was reduced to 7.68 kJ mol^{-1}. The E value further suggested that the Pb(II) removal by the FCC at initial pH 3.0 was a chemical nature (chemisorption/ion exchange), but the physical adsorption might be involved in Pb(II) removal at initial pH 6.0.[1,48]

In this work, the $q_{m,cal}$ of Pb(II) removal by the FCC reached 112.36 mg g^{-1} at initial pH 3.0 and at 25 °C. For the removal of Pb(II) ions, the maximum monolayer adsorption capacities of various adsorbents were given in Table 2. The adsorption capacity of the FCC was higher than that of carbon materials such as activated carbon and carbon nanotube, and close to that of iron–carbon composites. By considering the usage of cheap raw materials and solid waste in the fabrication of FCC, this novel microelectrolysis filter may be a promising sorbent in wastewater treatment.

3.4 Pb(II) removal in column experiments

Fig. 6 depicted the time-dependent evolution of Pb(II) removal by the FCC, AC and Fe^0/AC couples, respectively. The AC achieved the lowest removal of Pb(II). The breakthrough occurred at the fourth day and only 1.24% of Pb(II) removal was achieved after 12 days' run. This poor performance was attributed to low adsorption capacity of Pb(II) ions for unmodified AC as given in

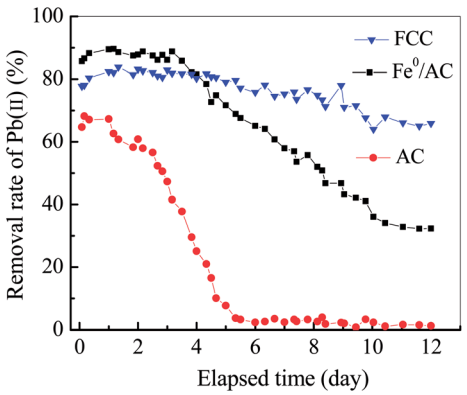

Fig. 6 Variation of removal rate of Pb(II) ions with elapsed time by Fe^0/C ceramsites (FCC), Fe^0 powders/activated carbon (Fe^0/AC) and activated carbon (AC).

Table 2.[49,50] In the first 4 days, the Pb(II) removal rate for Fe^0/AC couples was slightly higher than that for the FCC. For the FCC, the Fe^0 and carbon particles were embedded into ceramsites, the diffusion of Pb(II) ions from bulk solution to reactive sites in the inner surface of ceramsites must be limited. However, for Fe^0/AC couples, Fe^0 and AC particles were fully contacted with Pb(II) solutions, promoting significant removal of Pb(II) ions at initial stage. However, after 4 days, the Pb(II) removal rate for Fe^0/AC couples rapidly reduced. At the end of column test (12 days), the Pb(II) removal rate for Fe^0/AC couples was decreased to just 32.35%, but the value for the FCC was still as high as 65.86%. The result revealed that the FCC had good long-term run performance in the Pb(II) removal.

As shown in Fig. 4(b), the solution pH had increased from 6.0 at initial to 7.08 at equilibrium. The iron hydroxides must be formed in column tests as the precipitation of Fe(III) ions occurs even at pH 2.0–3.0 ($K_{sp} = 4.0 \times 10^{-38}$ for $Fe(OH)_3$ at 25 °C). For packed Fe^0/AC couples, the migration distance of $Fe(OH)_3$ colloids was short because the pore space of packed bed was very limited due to small particle size of Fe^0 particles, causing particle cementation and flow disturbance.[15,16] Nevertheless, the pore space in FCC packed bed was large enough to allow long distance migration of $Fe(OH)_3$ colloids due to large size (5 mm) of spheroidal FCC. Therefore, the cementation of FCC bed should be significantly alleviated, which supported high Pb(II) removal rate in 12 days' run. However, as seen in Fig. S4,† iron (red) and lead (white) (hydro)oxides were observed to be coated on FCC surface, which might hinder the mass transfer in Pb(II) removal process.

3.5 Lead removal mechanisms

3.5.1 XRD analysis. The XRD analysis was conducted to characterize crystalline phases of Fe^0/C ceramsites (FCC) after the Pb(II) removal. By comparing XRD patterns of the FCC before (see in Fig. 2) and after (see in Fig. 7) the Pb(II) removal, it was clear that two XRD patterns were quite different, indicating the occurrence of significant crystalline phase changes in the Pb(II) removal. The diffraction intensity of peaks assigned to Fe^0 remarkably decreased, showing the reduced content of metallic iron in the FCC after the removal of Pb(II). As shown in Fig. 7, the peaks with a 2θ degree at 15.04°, 29.07°, 30.29°, 32.56°, 37.81°, 49.14°, 50.69°, 53.11° corresponded to the (200), (111), (100), (020), (021), (202), (022) and (311) lattice planes of massicot (PbO), respectively. The peaks with a 2θ at 31.37°, 36.31°, 52.11°, 62.22° could be assigned to the (111), (200), (220) and (311) lattice planes of metallic lead (Pb^0), respectively. In addition, asisite ($Pb_7O_8Cl_2$), plumbojarosite ($Pb(Fe_3(OH)_6(SO_4)_2)_2$) and iron oxyhydroxide (α-FeOOH) were also presented with a lower fraction. By comparing the diffraction intensity of these crystals, it could find that the PbO was dominant Pb containing species.

The formation of Pb^0 suggested that Pb(II) ions could be removed *via* the reduction of Pb(II) to Pb^0 by the FCC. Since the standard reduction potential of Pb(II)/Pb^0 (−0.1263 V) is more positive than that of Fe(II)/Fe^0 (−0.4402 V),[57] Pb(II) can be reduced to Pb^0 by the Fe^0 *via* the electrochemical reaction. This result coincided well with previous studies in which Pb^0 was formed by presenting n-ZVI in Pb(II) solution.[11,58] As the corrosion of microscale Fe^0 embedded in the FCC could be enhanced with the galvanic couple effect of Fe^0 and carbon, released Fe(II) ions could coexist with Pb(II) ions in bulk solution. Because of their close K_{sp} (1.2×10^{-15} for $Pb(OH)_2$, 8.0×10^{-16} for $Fe(OH)_2$ at 25 °C) and neutral solution pH (above 7.0), Fe(II) and Pb(II) ions were (co-)precipitated to generate hydroxides on both internal and exterior surface of the FCC. In the previous studies,

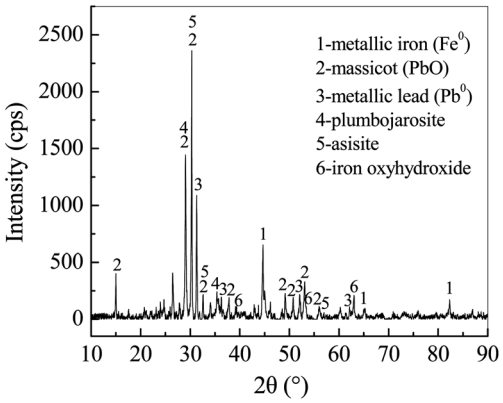

Fig. 7 XRD pattern of Fe^0/C ceramsites in the removal of Pb(II) ions after 12 days.

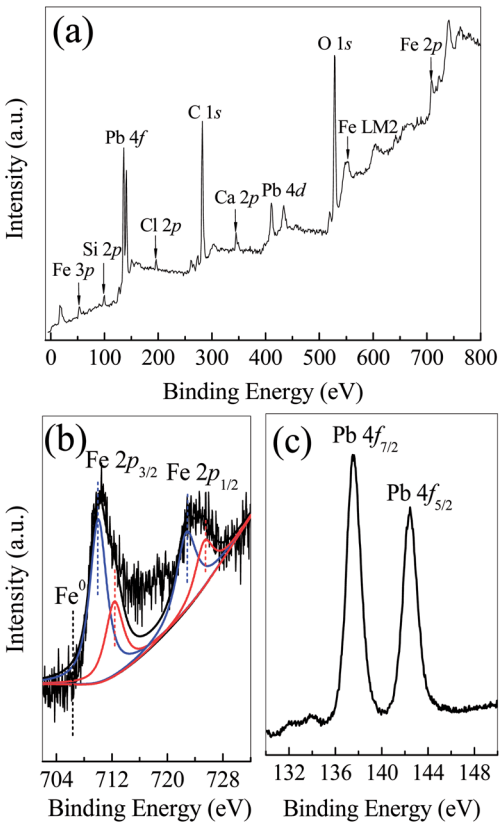

Fig. 8 XPS analysis of Fe^0/C ceramsites in the removal of Pb(II) ions after 12 days: wide-scan survey (a) and high-resolution XPS lines of Fe 2p (b) and Pb 4f (c).

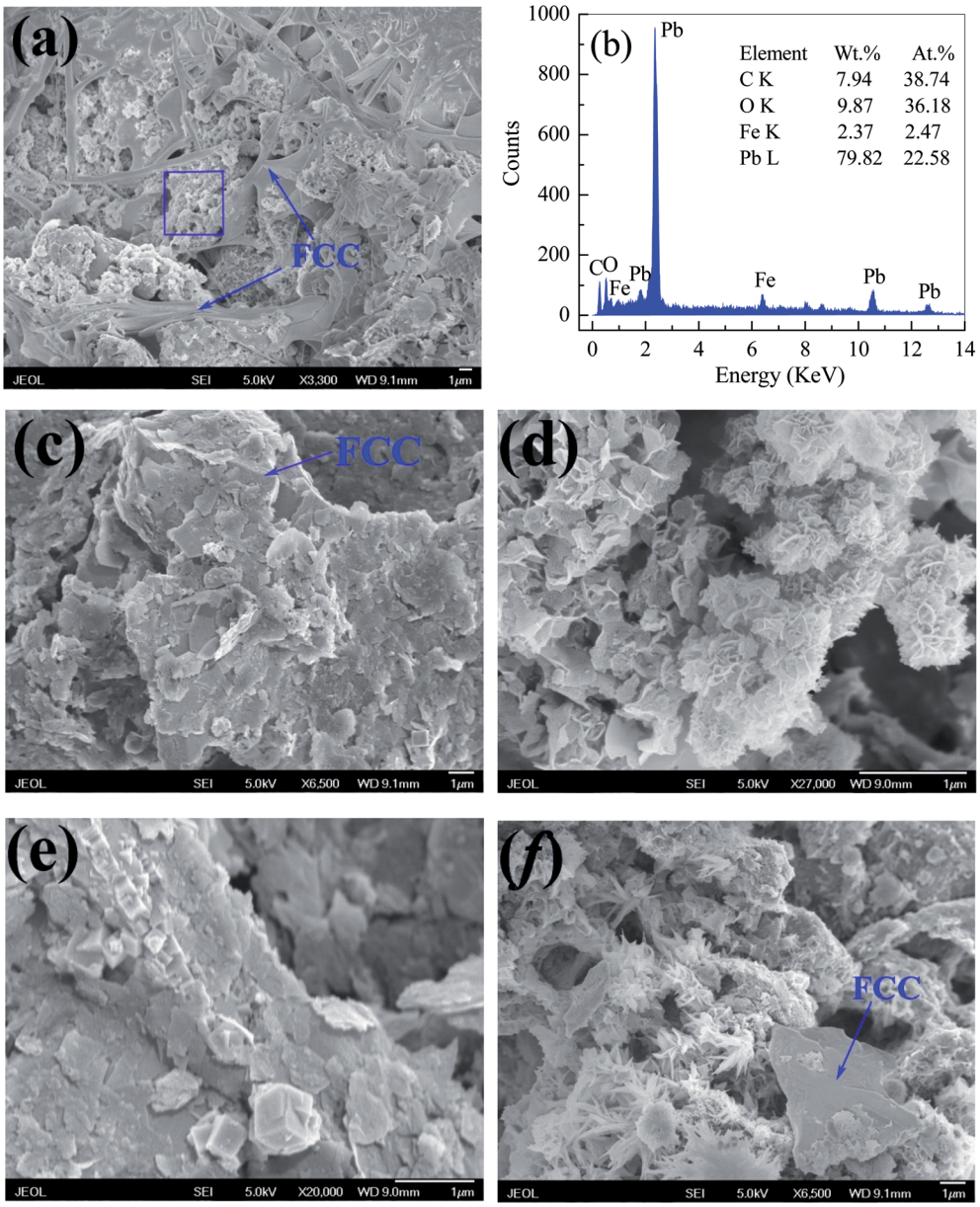

Fig. 9 SEM images of Fe^0/C ceramsites after the Pb(II) removal for 12 days and the EDX spectrum at selected area.

amorphous $Pb(OH)_2$ was observed on supported n-ZVI composites,[58,59] and cerussite ($Pb(CO_3)_2$) appeared on biochars.[60] But no characteristic peak of lead hydroxides and cerussite appeared in Fig. 7. The thermogravimetric analysis (TGA) had demonstrated that the decomposition temperature of cerussite to PbO and of $Pb(OH)_2$ to PbO were 223–361 °C and <160 °C, respectively.[60,61] Therefore, in this work, thermodynamically unstable $Pb(OH)_2$ might be formed as an intermediate which was subsequently transformed into stable PbO *via* dehydration in sample heating process.[59] The presence of PbO and Pb^0 as final products indicated that the (co-)precipitation and reduction occurred in the Pb(II) removal by the FCC.

3.5.2 XPS analysis. XPS analysis was conducted to reveal chemical states of Fe and Pb elements on Fe^0/C ceramsites (FCC) after the Pb(II) removal. As shown in Fig. 8(a), the elements of Fe, O, Pb, C, Si, Cl and Ca were observed. The high peak intensity of Pb 4f, C 1s and O 1s exhibited the high content of these elements on FCC surface. The high-resolution Fe 2p spectrum (Fig. 8(b)) could be deconvoluted into four peaks at 710.1, 712.3, 722.9 and 725.5 eV. The peaks at 725.5 and 722.9 eV corresponded to the binding energy of $2p_{1/2}$ of Fe(III) and Fe(II) species, respectively.[62,63] The peaks at 712.3 and 710.2 eV could be assigned to the $2p_{3/2}$ of Fe(III) and Fe(II) species, respectively.[64] The result showed the coexistence of Fe(III) and Fe(II) species on the FCC surface. However, no peak at around 706.0 eV was observed, indicating the disappearance of Fe^0 on FCC surface after Pb(II) removal.[2] Since the presence of Fe^0 in the FCC after Pb(II) removal was proved by XRD analysis, it clearly indicated that Fe^0 particles on FCC surface were completely corroded to release Fe(II) and Fe(III) ions into solution.

The high-resolution Pb 4f spectrum was illustrated in Fig. 8(c). Two main peaks at 137.7 and 142.6 eV could be assigned to binding energies of $4f_{7/2}$ and $4f_{5/2}$ of PbO, respectively.[65] No any characteristic peak of Pb^0 was observed. The lead species formed by n-ZVI had been quantitatively investigated with a sequential extraction procedure, which revealed a core–shell structure with Pb^0 and Fe^0 as the inner core and with PbO as the external shells.[66] While most of active sites of Fe^0 particles in the FCC were covered with the shells, the reduction of Pb(II) to Pb^0 might cease.

3.5.3 FESEM/EDX analysis. Fig. 9 showed FESEM/EDX observations for morphologies and elemental constitutions of the FCC after Pb(II) removal for 12 days. As illustrated in Fig. 9(a), ridge-like structures were original FCC materials. Some agglomerates, consisting of much smaller particles, were accumulated into the pores of these ridges. As revealed by EDX analysis at selected area (Fig. 9(b)), these agglomerates were mainly composed with Pb, O and C elements with a low proportion of Fe. As demonstrated by XRD and XPS analysis, the PbO was dominant Pb containing species on the FCC. Therefore, observed agglomerates should be mainly composed of PbO crystals due to extremely high content of Pb element. The Fe/C mass ratio of 0.298 : 1 at selected area was much lower than that of 7.5 : 1 in original FCC, which suggested that the Fe^0 was significantly corroded in the microelectrolysis reactions while remaining carbon (cathode) on FCC surface.

As shown in Fig. 9(c)–(f), PbO agglomerates had numerous structures of plate (c), flower (d), cuboid (e) and dentrite (f). Especially, a large amount of plate-like PbO particles was deposited on FCC surface in Fig. 8(c) and (e). Actually, PbO with plentiful structures, such as plate and dentrite, can be formed in the precipitation.[67,68] Since lots of PbO particles were coated on the inner and exterior surface of the FCC, it could reasonably infer that the precipitation of PbO might be a key pathway in removal of Pb(II) ions by the FCC.

3.5.4 Proposed mechanisms of Pb(II)removal. Compared to n-ZVI, microscale Fe^0 was much less active and very hard to be oxidized by Pb(II) and H_2O.[66] Nevertheless, by forming galvanic couples between Fe^0 and carbon, microscale Fe^0 in the FCC was readily corroded to release Fe(II) and to deplete H^+ ions, which promoted subsequent Pb(II) removal. As shown in Fig. 10, the removal of Pb(II) ions by the FCC might involve four pathways: (1) the reduction of Pb(II) to Pb^0 by Fe^0; (2) the precipitation of PbO; (3) formation of Pb containing compounds such as asisite and plumbojarosite by reacting with Cl^-, SO_4^{2-} and Fe(III) ions; (4) ion exchange with generated iron hydroxides (eqn (9) and (10)).[14]

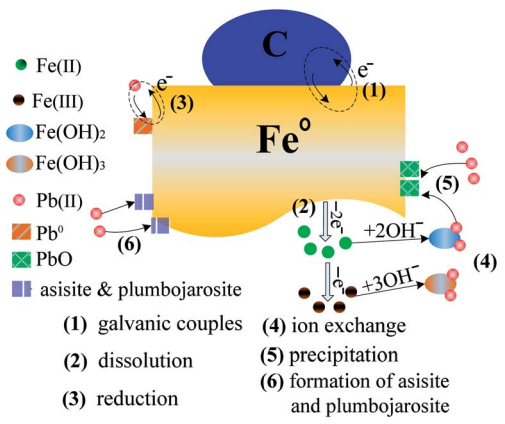

Fig. 10 Proposed mechanism in removing Pb(II) ions from aqueous solution by Fe^0/C ceramsites.

$$Fe(OH)_2 + Pb^{2+} \rightarrow Fe(OH)OPb^+ + H^+ \quad (9)$$

$$Fe(OH)_3 + Pb^{2+} \rightarrow Fe(OH)_2OPb^+ + H^+ \quad (10)$$

4. Conclusions

Porous Fe^0/C ceramsites (FCC), with the integrated structure of Fe^0 (anode) and carbon (cathode) of a microelectrolysis filter, were fabricated from magnetite, coal and paper mill sludge. Batch tests had demonstrated that the Pb(II) removal by the FCC was pH-sensitive with the increase of Pb(II) removal from 74.94% to 95.97% as initial pH was raised from 2.0 to 6.0. The equilibrium data at initial pH 3.0 was well fitted by the Langmuir isotherm, but the data obtained at initial pH 6.0 could be described by the Freundlich model. The precipitation of PbO resulted in multilayer adsorption of Pb species on the FCC as the pH increased from 6.0 to above 7.0. The maximum Pb(II) adsorption capacity of the FCC reached 112.36 mg g^{-1} at initial pH 3.0 and at 25 °C. Column tests showed that the FCC achieved the highest Pb(II) removal of 65.86% after 12 days' run compared to 32.35% for Fe^0/AC couples and only 1.24% for AC.

The XRD and XPS analysis revealed that the PbO (dominant Pb species), Pb^0, asisite and plumbojarosite appeared on the FCC after Pb(II) removal. The FESEM examination exhibited that PbO particles, with various structures of plate, flower, cuboid and dentrite, were accumulated on the FCC surface. The XRD, XPS and EDX analysis exhibited the remarkable decrease of metallic iron content in the FCC after the Pb(II) removal, revealing the effective corrosion of microscale Fe^0 by forming galvanic couples between Fe^0 and carbon. The Pb(II) removal by the FCC might involve reduction, precipitation, ion exchange and formation of Pb containing compounds by reacting with Cl^-, SO_4^{2-} and Fe(III) ions in bulk solution.

Conflicts of interest

There are no conflicts to declare.

Acknowledgements

This work was supported by the National Natural Science Foundation of China (No. 51674017) and the State Scholarship Fund of China Scholarship Council (No. 201706465070).

References

1 A. M. Azzam, S. T. EI-Wakeel, B. B. Mostafa and M. F. EL-Shahat, *J. Environ. Chem. Eng.*, 2016, **4**, 2196–2206.
2 J. Wang, G. J. Liu, T. F. Li and C. C. Zhou, *RSC Adv.*, 2015, **5**, 29859–29871.
3 R. Miehr, P. G. Tratnyek, J. Z. Bandstra, M. M. Scherer, M. J. Alowitz and E. J. Bylaska, *Environ. Sci. Technol.*, 2004, **38**, 139–147.
4 R. A. Crane and T. B. Scott, *J. Hazard. Mater.*, 2012, **211**, 112–125.
5 C. Noubactep, *Korean J. Chem. Eng.*, 2012, **29**, 1050–1056.
6 C. R. Keenan, R. Goth-Goldstein, D. Lucas and D. L. Sedlak, *Environ. Sci. Technol.*, 2009, **43**, 4555–4560.
7 K. Miyajima and C. Noubactep, *Chem. Eng. J.*, 2015, **262**, 891–896.
8 Y. Ren, J. F. Zhou, B. Lai, W. J. Tang and Y. Zeng, *RSC Adv.*, 2016, **6**, 108229–108239.
9 I. Mikhailov, S. Komarov, V. Levina, A. Gusev, J. P. Issi and D. Kuznetsov, *J. Hazard. Mater.*, 2017, **321**, 557–565.
10 X. M. Dou, R. Li, B. Zhao and W. Y. Liang, *J. Hazard. Mater.*, 2010, **182**, 108–114.
11 L. Yuan, W. Zhi, Q. L. Xie, X. Chen and Y. S. Liu, *Environ. Sci.: Water Res. Technol.*, 2015, **1**, 814–822.
12 B. Lai, Y. X. Zhou, P. Yang, J. H. Yang and J. L. Wang, *Chemosphere*, 2013, **90**, 1470–1477.
13 D. Y. Huang, Q. Y. Yue, K. F. Fu, B. J. Zhang, B. Y. Gao, Q. Li and Y. Wang, *Desalin. Water Treat.*, 2016, **57**, 4420–4428.
14 H. Modin, K. M. Persson, A. Andersson and M. van Praagh, *J. Hazard. Mater.*, 2011, **189**, 749–754.
15 A. Hussam and A. K. M. Munir, *J. Environ. Sci. Health, Part A: Toxic/Hazard. Subst. Environ. Eng.*, 2007, **42**, 1869–1878.
16 C. Noubactep, *Chemosphere*, 2014, **117**, 104–107.
17 R. H. Yang, J. Z. Zhu, Y. L. Li and H. Zhang, *Int. J. Environ. Res. Public Health*, 2016, **13**, 457–471.
18 V. K. Gupta, A. Nayak and S. Agarwal, *Environmental Engineering Research*, 2015, **20**, 1–18.
19 T. A. Saleh and V. K. Gupta, *Adv. Colloid Interface Sci.*, 2014, **211**, 93–101.
20 V. K. Gupta and T. A. Saleh, *Environ. Sci. Pollut. Res.*, 2013, **20**, 2828–2843.
21 R. X. Bai, Y. Zhang, Z. G. Zhao, Q. X. Liao, P. Chen, P. P. Zhao, W. H. Guo, F. Yang and L. C. Li, *J. Ind. Eng. Chem.*, 2018, **59**, 416–424.
22 L. Yuan, W. Zhi, Y. Liu, S. Karyala, P. J. Vikesland, X. Chen and H. S. Zhang, *Environ. Sci. Technol.*, 2015, **49**, 824–830.
23 M. Ahmaruzzaman and V. K. Gupta, *Ind. Eng. Chem. Res.*, 2011, **50**, 13589–13613.
24 D. C. Bellinger, *Int. J. Environ. Res. Public Health*, 2011, **8**, 2593–2628.
25 C. F. Carolin, P. S. Kumar, A. Saravanan, G. J. Joshiba and M. Naushad, *J. Environ. Chem. Eng.*, 2017, **5**, 2782–2799.
26 S. Suganya and P. S. Kumar, *J. Ind. Eng. Chem.*, 2018, **60**, 418–430.
27 P. S. Kumar, R. Sivaranjanee, P. S. Rajan and A. Saravanan, *J. Ind. Eng. Chem.*, 2018, **60**, 307–320.
28 E. Gunasundari and P. S. Kumar, *IET Nanobiotechnol.*, 2017, **11**, 317–328.
29 H. Sharififard, F. Pepe, M. Soleimani, P. Aprea and D. Caputo, *RSC Adv.*, 2016, **6**, 42845–42853.
30 A. R. Kaveeshwar, S. K. Ponnusamy, E. D. Revellame, D. D. Gang, M. E. Zappi and R. Subramaniam, *Process Saf. Environ. Prot.*, 2018, **114**, 107–122.
31 E. Gunasundari and P. S. Kumar, *J. Ind. Eng. Chem.*, 2017, **56**, 129–144.
32 N. Mohammadi, H. Khani, V. K. Gupta, E. Amereh and S. Agarwal, *J. Colloid Interface Sci.*, 2011, **362**, 457–462.
33 H. Shafiififard, F. Z. Ashtiani and M. Soleimani, *Asia-Pac. J. Chem. Eng.*, 2013, **8**, 384–395.
34 V. K. Gupta, A. Nayak, S. Agarwal and I. Tyagi, *J. Colloid Interface Sci.*, 2014, **417**, 420–430.
35 D. Robati, B. Mirza, M. Rajabi, O. Moradi, I. Tyagi, S. Agarwal and V. K. Gupta, *Chem. Eng. J.*, 2016, **284**, 687–697.
36 G. S. Liu, V. Strezov, J. A. Lucas and L. J. Wibberley, *Thermochim. Acta*, 2004, **410**, 133–140.
37 F. Ju and Y. Y. Hu, *Sep. Purif. Technol.*, 2011, **78**, 33–41.
38 J. W. Liu, T. Mwamulima, Y. M. Wang, Y. Fang, S. X. Song and C. S. Peng, *J. Mol. Liq.*, 2017, **243**, 205–211.
39 P. Wu and Y. S. Zhou, *J. Hazard. Mater.*, 2009, **168**, 674–680.
40 H. Genc-Fuhrman, P. Wu, Y. S. Zhou and A. Ledin, *Desalination*, 2008, **226**, 357–370.
41 V. K. Gupta, R. Kumar, A. Nayak, T. A. Saleh and M. A. Barakat, *Adv. Colloid Interface Sci.*, 2013, **193–194**, 24–34.
42 M. Ghaedi, S. Hajjati, Z. Mahmudi, I. Tyagi, S. Agarwal, A. Maity and V. K. Gupta, *Chem. Eng. J.*, 2015, **268**, 28–37.
43 A. Asfaram, M. Ghaedi, S. Agarwal, I. Tyagi and V. K. Gupta, *RSC Adv.*, 2015, **5**, 18438–18450.
44 P. S. Kumar, A. Saravanan, K. A. Kumar, R. Yashwanth and S. Visvesh, *IET Nanobiotechnol.*, 2016, **10**, 244–253.
45 G. Neeraj, S. Krishnan, P. S. Kumar, K. R. Shriaishvarya and V. V. Kumar, *J. Mol. Liq.*, 2016, **214**, 335–346.
46 A. Mittal, J. Mittal, A. Malviya and V. K. Gupta, *J. Colloid Interface Sci.*, 2010, **344**, 497–507.
47 Y. M. Hao, M. Chen and Z. B. Hu, *J. Hazard. Mater.*, 2010, **184**, 392–399.
48 L. Yuan and Y. S. Liu, *Chem. Eng. J.*, 2013, **215**, 432–439.
49 M. E. Lee, J. H. Park, J. W. Chung, C. Y. Lee and S. Kang, *J. Ind. Eng. Chem.*, 2015, **21**, 470–475.
50 T. Depci, A. R. Kul and Y. Onal, *Chem. Eng. J.*, 2012, **200**, 224–236.
51 Z. B. Bouabidi, M. H. El-Naas, D. Cortes and G. McKay, *Chem. Eng. J.*, 2018, **334**, 837–844.
52 N. D. V. Quyen, T. N. Tuyen, D. Q. Khieu, H. V. M. Hai, D. X. Tin, P. T. N. Lan and I. Kiyoshi, *Bull. Mater. Sci.*, 2018, **41**, 6.
53 W. J. Zhang, Y. C. Zhang, Y. Gutha and J. Xu, *Int. J. Biol. Macromol.*, 2017, **105**, 422–430.
54 F. C. Christopher, S. Anbalagan, P. S. Kumar, S. R. Pannerselvam and V. K. Vaidyanathan, *IET Nanobiotechnol.*, 2017, **11**, 433–442.

55 S. Anbalagan, S. K. Ponnusamy, S. R. P. Selvam, A. Sankaranarayan and A. Dutta, *Korean J. Chem. Eng.*, 2016, **33**, 2716–2731.
56 S. Suganya, A. Saravanan, P. S. Kumar, M. Yashwanthraj, P. S. Rajan and K. Kayalvizhi, *IDA J. Desalin. Water Reuse*, 2017, **7**, 214–227.
57 Y. L. Zhang, Y. M. Li, J. F. Li, G. D. Sheng, Y. Zhang and X. M. Zheng, *Chem. Eng. J.*, 2012, **185**, 243–249.
58 X. Zhang, S. Lin, Z. L. Chen, M. Megharaj and R. Naidu, *Water Res.*, 2011, **45**, 3481–3488.
59 M. H. Liu, Y. H. Wang, L. T. Chen, Y. Zhang and Z. Lin, *ACS Appl. Mater. Interfaces*, 2015, **7**, 7961–7969.
60 Z. T. Shen, Y. Y. Zhang, F. Jin, O. McMillan and A. Al-Tabbaa, *Sci. Total Environ.*, 2017, **609**, 1401–1410.
61 S. A. A. Sajadi, A. A. Alamolhoda and S. J. Hashemian, *Sci. Iran.*, 2007, **14**, 169–173.
62 Z. Li, H. Chen, H. B. Bao and M. Y. Gao, *Chem. Mater.*, 2004, **16**, 1391–1393.
63 H. L. Peng, Z. Y. Mo, S. J. Liao, H. G. Liang, L. J. Yang, F. Luo, H. Y. Song, Y. L. Zhong and B. Q. Zhang, *Sci. Rep.*, 2013, **3**, 1765.
64 P. Marcus and J. M. Grimal, *Corros. Sci.*, 1992, **33**, 805–814.
65 S. S. Barala, B. Roul, N. Banerjee and M. Kumar, *J. Appl. Phys.*, 2016, **120**, 115305.
66 N. M. Zhu, Y. S. Xu, L. C. Dai, Y. F. Zhang and G. Q. Hu, *J. Hazard. Mater.*, 2018, **351**, 138–146.
67 K. C. Chen, C. W. Wang, Y. I. Lee and H. G. Liu, *Colloids Surf., A*, 2011, **373**, 124–129.
68 P. B. Taunk, R. Das, D. P. Bisen and R. K. Tamrakar, *Optik*, 2016, **127**, 6028–6035.